Circularly Polarized Light Induced Microwave Conductivity Measurement: Rapid Screening Technique of Electronic Conductivity in Chiral Molecular Materials

Yun Hee Koo[1], *Yusuke Tsutsui*[1,2,*], *Mikito Omoto*[3], *Yohei Yomogida*[4], *Kazuhiro Yanagi*[3,5,*], *Yuichiro K. Kato*[6,7], *M. Alejandra Hermosilla-Palacios*[8], *Jeffrey L. Blackburn*[8,*], *and Shu Seki*[1,4,*]

[1]Department of Molecular Engineering, Kyoto University, Kyoto University Katsura, Nishikyo-ku, Kyoto 615-8510, JAPAN

[2]JST-PRESTO, Honcho 4-1-8, Kawaguchi, Saitama 332-0012, Japan

[3]Department of Physics, Graduate School of Science, Tokyo Metropolitan University, 1-1 Minami-Osawa, Hachioji-shi, Tokyo 192-0397, JAPAN

[4] Research Institute for Electronic Science, Hokkaido University, Sapporo, Hokkaido 001-0021, Japan

[5]JST-CREST, Honcho 4-1-8, Kawaguchi, Saitama 332-0012, Japan

[6]Nanoscale Quantum Photonics Laboratory, RIKEN Cluster for Pioneering Research, Saitama 351-0198, JAPAN

[7]Quantum Optoelectronics Research Team, RIKEN Center for Advanced Photonics, Saitama 351-0198, JAPAN

[8]National Renewable Energy Laboratory, 15013 Denver West Parkway Golden, CO 80401, USA

AUTHOR INFORMATION

Corresponding Author

tsutsui@moleng.kyoto-u.ac.jp; yanagi-kazuhiro@tmu.ac.jp; Jeffrey.Blackburn@nrel.gov; seki@moleng.kyoto-u.ac.jp

ABSTRACT

We developed CPL-TRMC (Circularly Polarized Light-Time Resolved Microwave Conductivity) for investigation of the CPL-dependent photo-induced charge carrier dynamics in chiral materials with chiroptical properties. Chiral *R*- or *S*-perylenediimide (PDI) molecular thin films were paired with handedness-sorted (6,5) and (11,-5) single-walled carbon nanotube (SWCNT) films to compose donor(D)-acceptor(A) system for spin-dependent charge separation process, and the D-A system was examined through linear and circular polarization dependent steady-state and time-resolved measurements. The *R*-PDI-(6,5) film exhibited strong enhancement in circular dichroism (CD), and revealed a reversed transient conductivity signal, relative to the polarity of CD, in CPL-TRMC measurement upon excitation of the E_{11} state, which is interpreted as arising from a spin-dependent initial charge separation process. Through linear polarization dependent flash photolysis TRMC and circular polarization resolved femtosecond transient absorption, we could deduce that sub-ps inter-tubular charge separation upon E_{11} excitation in SWCNT was responsible for the spin-dependent photoconductivity transients observed in CPL-TRMC measurements.

TOC GRAPHICS

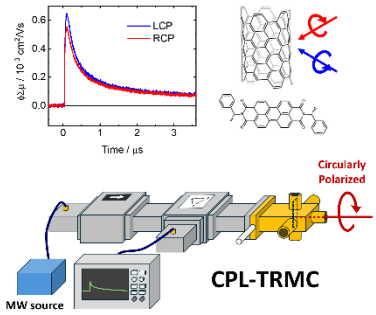

KEYWORDS Circularly Polarized Light, Chirality, Carbon Nanotube, Microwave, Conductivity

Recent developments in spintronics shed light on chiral materials for the application of electron spins as well as the spin-dependent charge transport. Various types of chiral materials encompassing biological systems, synthetic organic and inorganic chemistry have been suggested, and their charge/spin transport properties were examined through several different spin injection methods.[1-4] Spin injection by ferromagnetic electrodes is a primary choice in spintronic device operation, and a variety of structures have been designed to enable efficient and quantitative spin injection into target materials.[5] Adopting ferromagnetic electrodes for spin injection requires device fabrication processes, and interfacial issues between ferromagnets and target materials are often critical for optimizing device operation.[6-7]

Photoionization by circularly polarized light (CPL) can be utilized for contact-free spin injection into target materials through spin-dependent excitation of the electrons.[8-9] Spin-polarized photoelectron spectroscopy (PES) under CPL illumination has been used to evaluate the spin selectivity of electrons transmitted through chiral materials, and photo-current measurement under

CPL illumination has been often the choice for spin-selective transport and spin-selective charge transfer in chiral organic and inorganic materials.[1, 10-11] In both of the techniques the contact issues are critical to the quantitative assessment of spin selectivity and transport, leading to strong demand for alternative methods utilizing non-contact modes.

Time-resolved spectroscopy techniques with CPL excitation have been demonstrated as complete non-contact assessments of spin-dependent charge transport chiral materials and heterostructures. Dependence of charge transfer rate on spin-selective excitation was clearly observed using a time-resolved fluorescence (TR-FL).[12] The spin polarization of radical pairs formed by electron transfer could be calculated using the time-resolved electron paramagnetic resonance (TR-EPR) spectroscopic system in donor-acceptor dyad systems with chiral components.[13] These recently developed spectroscopic approaches can reveal mechanistic insights into the spin-dependent charge transfer processes. For comprehensive understanding of the total landscape of spin-dependent charge transfer processes, direct methods for tracking the local motion of the electrons with high sensitivity are highly desirable.[14]

Electronic conductivity can be measured not only by conventional direct current (DC) techniques, but also as optical conductivity in terms of a material's complex permittivity. One of the representative optical conductivity techniques is the time resolved microwave conductivity (TRMC) technique, based on Drude-Zhener modeling of the frequency dependent dielectric constant.[15] Flash photolysis (FP)-TRMC is a completely contactless technique, both in the photo-carrier injection step and for monitoring the resulting electrical conductivity with the microwave probe.[16-18] Herein, we employ CPL as an excitation light source to design a novel contactless technique for assessing inherent spin-dependent electron transport, which we term CPL-induced time-resolved microwave conductivity (CPL-TRMC).

Donor-acceptor heterojunctions featuring single-walled carbon nanotubes (SWCNTs) with single chirality and handedness were chosen for demonstration of the CPL-TRMC system, owing to their high conductivity, well-defined handedness, and concomitant distinct optical anisotropy in their electronic transitions. Electronic transitions of chirality sorted SWCNT can be predicted from the chirality indices (*n,m*) of the SWCNTs and pure enantiomers show, both theoretically and experimentally, alternating CD signs upon progression of E_{ii} transitions which are optically allowed transitions for the electric field of the light parallel to the axis of the nanotube.[19-20] SWCNTs can give strong TRMC signals upon photoexcitation via the direct band-gap excitation, the prerequisite for CPL-TRMC in the present work, due to the relatively large Onsager distance for the initial electron-hole pairs in SWCNT and a high free charge carrier yield of ~6% in isolated semiconducting SWCNTs.[21] The high carrier mobilities in SWCNTs should allow us to detect evident signatures of CPL excitation in the differential transient conductivity.[22-23] Successful demonstration of spin-dependent charge separation upon CPL illumination of a SWCNT/perovskite bilayer further suggests the possibility of detecting spin-dependent charge separation with CPL-TRMC.[11]

In this work, we demonstrate the successful establishment of the CPL-TRMC measurement system with SWCNT as a material platform, showing spin-dependent charge transfer in the SWCNTs. The total landscape of charge-spin relationship in SWCNT film upon charge injection through CP photoexcitation has been elucidated by the combination of CPL-TRMC and femtosecond transient absorption.

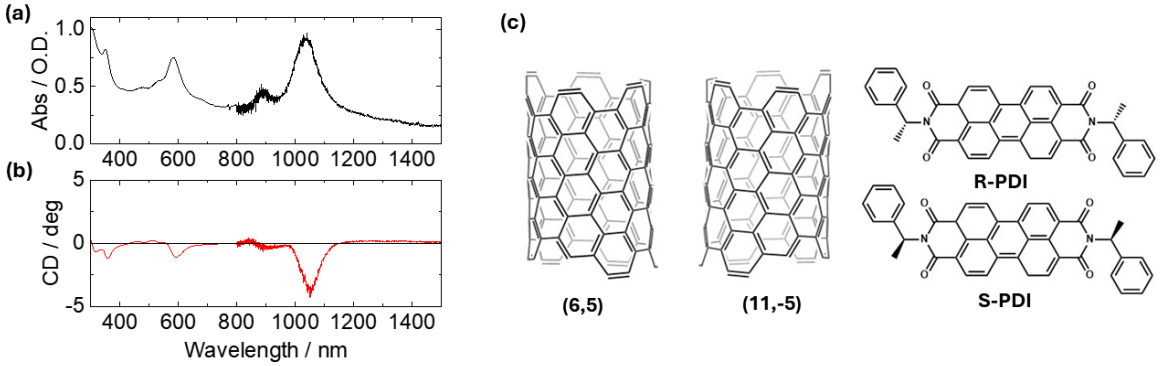

Figure 1. The steady-state (a) absorption and (b) circular dichroism (CD) spectra of *R*-PDI-(6,5) SWCNT film. 50 μL of *R*-PDI 1 mg/mL tetrahydrofuran solution was drop-casted to pristine (6,5) film to produce *R*-PDI-(6,5) film. (c) structures of (6,5) and (11,-5) SWCNT and *R*/*S*-PDI.

Design of a photo-induced charge transfer system is the key for the measurements where the electrons are unidirectionally transferred under the electrochemical potentials with no external electric field, allowing pure spectroscopic assessment of chirality-induced spin selectivity.[14] To facilitate the charge transfer, we chose perylenediimide (PDI) as the electron acceptor which is expected to form type-II heterojunction with (6,5) and (11,-5) SWCNTs ((6,5)- and (6,5)+ or left- and right-handed (6,5)).[24] We also adopted chiral *R*/*S*-PDI to examine their interaction with handedness-sorted SWCNT films, with an exemplary heterojunction referred to as *R*-PDI-(6,5). The chirality of both the donor (SWCNT) and acceptor (PDI) allows us to investigate how their structural and electronic interactions, and the resulting photoexcited interfacial charge transfer, depend on their chirality combination.

Figure 1a shows steady-state UV-vis-IR absorption for the *R*-PDI-(6,5) film. The allowed optical transitions from electric field parallel to the SWCNT axis: E_{ii} were observed at 1030, 580, 350 nm for E_{11}, E_{22}, and E_{33}, respectively. The former two peaks showed bathochromic shifts in relation

to those observed in the isolated (6,5) SWCNT with E_{11} and E_{22} transitions at 975 and 567 nm.[25] These shifts could be attributed to the bundling of the carbon nanotubes in the film.[26] The circular dichroism (CD) spectra (Figure 1b) showed three negative peaks at similar peak positions to the absorption spectrum, where the maximum value reached ca. 4×103 mdeg. The difference in the absorption between left-handed circularly polarized light (LCPL) and right-handed circularly polarized light (RCPL) of *R*-PDI-(6,5) film was calculated to be 12% at E_{11} transition, which is significantly higher than the 0.33% difference in the pristine (11,-5) film (Figure S1c). Only this specific R-PDI-(6,5) film shows strong enhancement in the CD peaks at E_{11}, E_{22}, and E_{33} transitions compared to the corresponding pristine SWCNT film, while other *R*-PDI or *S*-PDI deposited SWCNT films did not show such a strong CD enhancement (Figure S1d, S3c,d). The possibility of apparent CD effect, which is an extrinsic CD effect from sample morphology was examined in pristine (6,5) and (11,-5) film. (Figure S4)[27] Apparent CD effect was not observed, yielding identical CD spectra for front and back side of the pristine (6,5) and (11,-5) film. This lack of the apparent CD effect can be explained by randomness of the orientation of SWCNTs on the film and enhancement of the CD observed in R-PDI-(6,5) film is also expected to be not from apparent CD effect owing to the randomness of the SWCNT orientation in this film.

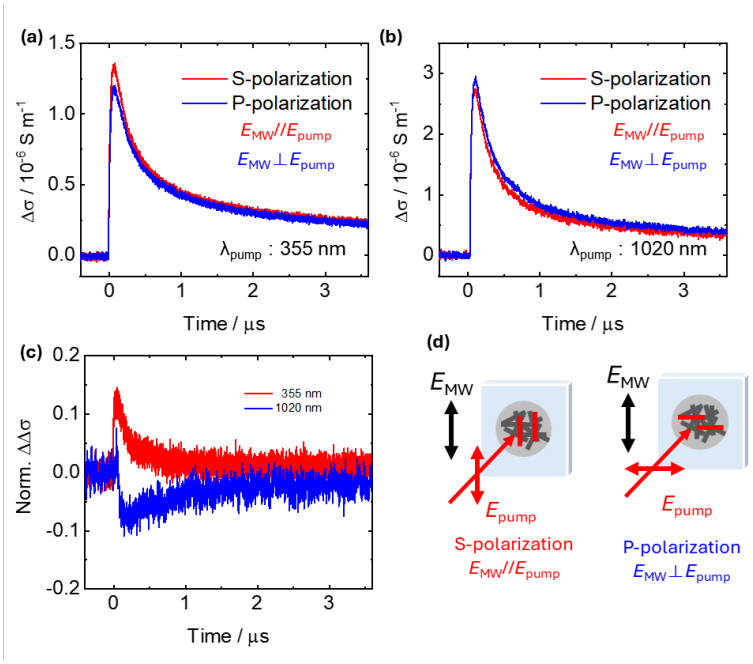

Figure 2. FP-TRMC traces of *R*-PDI-(6,5) SWCNT under (a) 355 (E_{33}) and (b) 1020 nm (E_{11}) excitation. (c) Differential conductivity transients normalized at the peak value. Linear polarization state of the excitation pulse was adjusted to S- (red) and P- (blue) polarization. The excitation pulse was tuned to 0.5 mJ pulse^{-1} cm^{-2} at 355 nm and 1 mJ pulse^{-1} cm^{-2} at 1020 nm, respectively. The relative orientation of the electric field for microwave (E_{MW}) and pump pulse (E_{pump}) is depicted in Figure 2d.

First, anisotropic photoconductivity in FP-TRMC was studied to clarify the charge carrier dynamics in the *R*-PDI-(6,5) film with linearly polarized excitation light sources and represented in Figure 2. Polarization of the excitation pulse was adjusted to be linear, and S- and P-polarizations of the pump pulse are defined as perpendicular and parallel polarization in relation to the optical table surface, respectively. The microwave electric field (E_{MW}) is perpendicular to the optical table surface, hence, S- and P- polarization of the pump is parallel and perpendicular to

the E_{MW}, respectively (Figure 2d). Both excitation wavelengths clearly showed a prompt enhancement in photoconductivity due to photo-carrier injection within the pump pulse (3-5 ns), followed by a decay in the μs range reflecting the recombination of the free charge carriers (Figure 2a, b). In the case of 355 nm excitation (E_{33}, Figure 2a), S-polarization pump resulted in slightly higher photoconductivity for the short time regime (<1 μs) and converged into equivalent photoconductivity at the later regime, indicating the decay of conductivity anisotropy (Figure 3a, c). The conductivity anisotropy reversed upon E_{11} (1020 nm) excitation of R-PDI-(6,5) with reduced anisotropy signals relative to E_{33} pumping. It should be noted that the conductivity anisotropy lasted over 3 μs regime (Figure 2b, c).

The conductivity anisotropy is impacted by the following relative alignments of E_{pump}, E_{MW}, and SWCNT axes: 1) The parallel alignment of SWCNT axes and E_{pump} enhances conductivity from selective excitation of SWCNT, 2) Photo-injected carriers confined in the SWCNT give the higher conductivity under the parallel alignment of E_{MW} and SWCNT axes. (Figure 2d) Since our SWCNT film is oriented randomly, the number of carbon nanotubes in the excited states can be presumed to be identical upon S- or P- polarization of light, cancelling the above factor 1) allowing us to consider only the relative alignments of E_{pump} against E_{MW}.

If charge generation occurs predominantly within a nanotube (intra-tubular), the charge movement and associated microwave mobility of photo-generated charge carriers confined within SWCNTs will remain aligned with E_{pump}, yielding a microwave conductivity anisotropy signal corresponding to S-polarization (E_{pump}//E_{MW} configuration). On the other hand, if inter-tubular charge separation and/or charge transfer to PDI dominate, conductivity anisotropy is expected to be lower than that of intra-tubular charge separation due to the randomization of the charged SWCNT axes. Exciton diffusion, prior to charge separation, and charge diffusion will

also suppress the anisotropy by transferring excitons and charges onto randomly oriented SWCNTs. In this manner, stronger S-polarization photoconductivity observed upon E_{33} excitation, compared to E_{11} excitation, can be interpreted as 1) a decrease in the exciton diffusion for E_{33} excitation, or 2) more efficient charge transfer to adjacent SWCNTs and/or PDI in the film for E_{11} excitation.

The photoconductivity anisotropies observed in Figure 2 imply that different CS pathways can be activated for different excitation wavelengths. From the ultrafast charge separation observed in fs-TA of SWCNT films (presented in a later section), we expect the above 1) process (exciton diffusion prior to charge separation) is not the dominant mechanism impacting the observed polarization anisotropies. Thus, the decrease in linear polarization conductivity anisotropy observed at FP-TRMC measurement in R-PDI-(6,5) film can be interpreted as activation of the inter-tubular CS or CS to PDI upon E_{11} excitation. The difference between E_{33} and E_{11} excitation in this film can be interpreted by the exciton dissociation process in SWCNT depending on E: the intra-tubular CS process dominates via the higher energy (E_{33} and E_{22}) excited state, making contrast to both of inter-tubular CS and CS to PDI contributing to the photo-carrier generation via the lower (E_{11}) excited state. Existence of spontaneous dissociation process from the higher excited state is expected to be contributing to the excitation wavelength dependence in the carrier yield and the CS pathway change.[28,29] This is also supported by the linear dependence of the observed conductivity upon fluence of pumping pulses (Figure S10), suggesting the nature of single photon process of CS in this fluence regime.

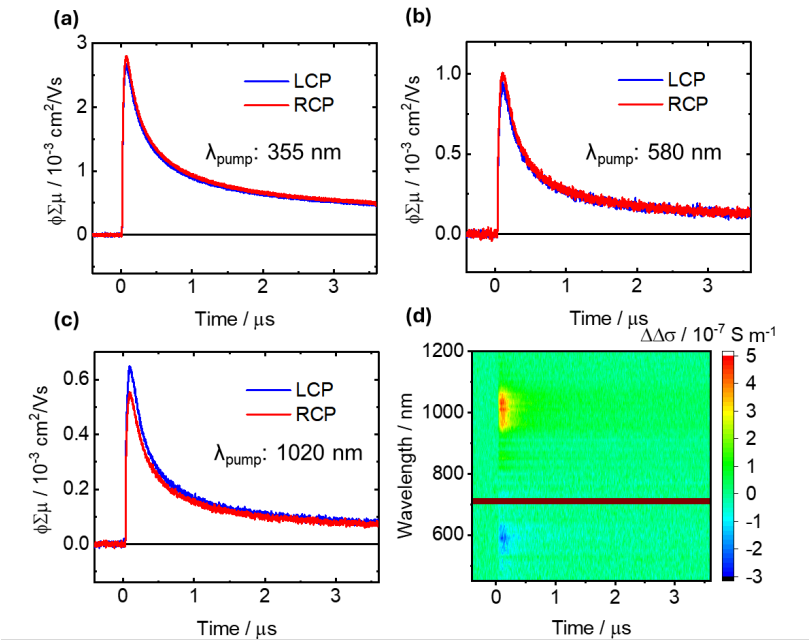

Figure 3. CPL-TRMC photoconductivity traces of the *R*-PDI-(6,5) film at (a) 355 nm: E_{33} (b) 580 nm: E_{22} (c) 1020 nm: E_{11} excitation. The excitation pulse was tuned to 0.5 mJ pulse^{-1} cm^{-2} at 355 nm and 1 mJ pulse^{-1} cm^{-2} at 580 and 1020 nm. Circular polarization state of the excitation pulse was adjusted to left-handed circular polarization (blue, LCP) and right-handed circular polarization (red, RCP). (d) Differential conductivity measured at the excitation wavelength range from 450 to 1200 nm.

In order to assess photo-generated electron spin-dependency upon CPL excitation of the *R*-PDI-(6,5) film, photoconductivity transients in the R-PDI-(6,5) film were observed by the newly developed CPL-TRMC measurement setup. The film was photo-excited at 355, 580, and 1020 nm which correspond to the E_{33}, E_{22} and E_{11} transitions of the (6,5)-SWCNT, where the PDI is transparent against 1020 nm, but presumed to have some overlapped absorption at 355 and 580 nm (Figure S2).

Upon E_{33} and E_{22} excitation, photoconductivity under RCPL excitation was higher than LCPL, and the difference in the LCPL and RCPL excitation at the peak was estimated to be 5% as represented by Figures 3a and 3b. This sign difference agrees with the difference in the relative absorption change of LCPL and RCPL estimated from CD (~5%). On the other hand, upon E_{11} excitation at 1020 nm (Figure 3c), remarkably higher photoconductivity of ca. 15% was observed with LCPL excitation, which showed striking contrast to the higher absorption of RCPL suggested by CD. Decay analysis of the photoconductivity traces was also conducted by fitting with double exponential decay curves to evaluate the time constant as summarized in Table 1. Regardless of the excitation wavelength and polarization, calculated time constants were estimated to be almost identical among all traces, with τ_1 and τ_2 of approximately 0.20 and 1.2 μs, implying the recombination rates unchanged for different wavelengths and circular polarization (CP) states of pumping pulses.

Table 1. Decay fitting coefficients of CPL-TRMC traces

λ_{exc} / nm		τ_1[a]/ μs	τ_2[a]/ μs	y_0 (%)	A_1 (%)	A_2 (%)
355	LCP	0.20	1.22	13.0	56.4	30.6
	RCP	0.20	1.20	12.8	56.6	30.6
580	LCP	0.20	1.18	10.4	61.5	28.0
	RCP	0.20	1.21	10.2	62.0	27.8
1020	LCP	0.20	1.23	10.2	64.5	25.2
	RCP	0.22	1.34	11.5	61.3	27.2

[a]Photoconductivity traces were fitted with the function $\varphi(t) \sum \mu = A_1 e^{t/\tau_1} + A_2 e^{t/\tau_2} + y_0$

Unlike direct injection of the spin-polarized charges through ferromagnetic electrodes, the spin-dependent CS process mediates the spin polarization of charge carriers that are *photo-injected* into a system. The yield and spin polarization of the charges are the major factors for the

CS processes, which can be determined by the rates of CS for up- ($k_{CS\uparrow}$) and down-spins ($k_{CS\downarrow}$), spin-flip (k_{flip}), and exciton relaxation to the ground state (k_F and k_n) as shown in Figure S9. The yield and spin-polarization of the photo-injected free charges thus depend strongly on the relative rate of competing processes. If the spin-flip process has a competitive rate with charge separation processes (i.e., $k_{flip} \sim k_{CS\uparrow}$ or $k_{CS\downarrow}$), the CS process with low rate constants can be impacted by the spin flipping, leading to the observable single CS. This also causes the final CS state to be condensed with the spin with the higher CS rate, and thus the spin polarization would not be identical to that in the primary excited states. This spin-flip process is widely observed in systems with chirality-induced spin selectivity (CISS); PES experiments with DNA embedded on gold show spin polarization almost identical from RCPL and LCPL excitation.[1] The primary photophysical process will be discussed in the later fs-TA section.

Since charge separation in the PDI-SWCNT composites is expected to be faster than the excitation pulse duration, we can only probe the impact of the pump-prepared spin polarization on CS by quantifying the total carrier yield and the recombination rate upon CPL excitation. The dependence of recombination rate, however, may not be significant because the spin polarization in the final CS states can be mitigated by spin-flipping at the primary excited states and by the spin relaxation after CS.

The values of end-of-pulse conductivity ($\phi\Sigma\mu_{max}$) depend clearly on the CPL states of the excitation pulse in all three wavelengths (Figure 3a-c). The $\phi\Sigma\mu_{max}$ values can be also impacted by 1) the number of the photons absorbed by the film with LCPL and RCPL excitation, and by 2) the spin-dependent CS processes via spin-selective excitation by LCPL and RCPL represented by $k_{CS\uparrow}$, $k_{CS\downarrow}$, k_F, k_n and/or k_{flip}. If this dependence solely comes from 1), photoconductivity traces should be proportional to the absorption of the LCPL and RCPL. This is well represented by the

cases of excitations at E_{33} and E_{22} supporting scenario 1). On the other hand, reversed polarity observed in E_{11} excitation opens the possibility of 2). This is also suggestive of the values of $\phi\Sigma\mu_{max}$ being more likely to convey the dependence of CS efficiency on the handedness of CPL excitation.

From the linear polarization experiment, we deduced that in *R*-PDI-(6,5) film, inter-tubular or charge separation to the PDI is promoted upon E_{11} compared to E_{33} excitation. Thus, the difference in CPL dependency upon excitation wavelength change in R-PDI-(6,5) film can be explained by the switching of CS pathways from the higher (E_{33} and E_{22}) to lower (E_{11}) excited state, and this change in CS pathway is expected to be responsible for the spin-dependent CS processes observed in CPL-TRMC.

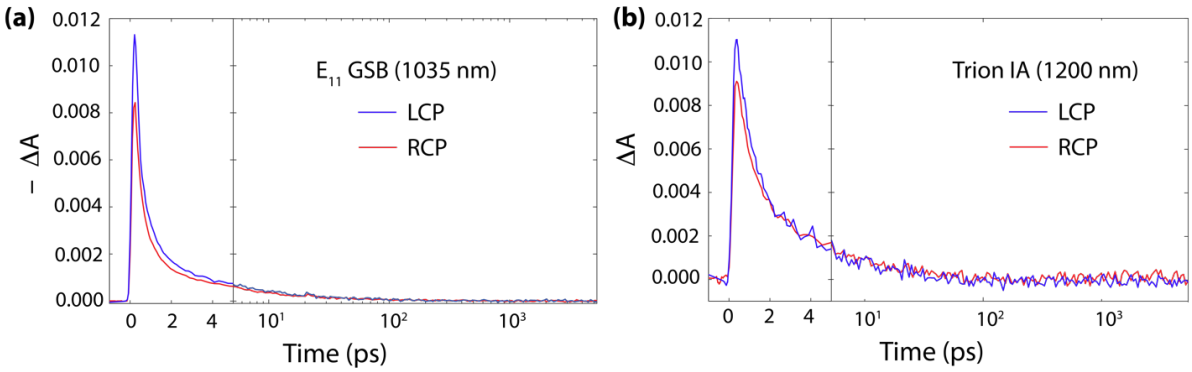

Figure 4. Dynamics from femtosecond transient absorption spectroscopy of the *R*-PDI-(6,5) film, pumped at 1000 nm to excited the (6,5) E_{11} with either a LCP (blue) or RCP pump (red) beam and probed with a linear probe beam. (a) Dynamics probed at 1035 nm to probe the E_{11} ground-state bleach (GSB). (b) Dynamics probed at 1200 nm to probe the trion induced absorbance (IA).

In order to elucidate the early photophysics of the *R*-PDI-(6,5) film, circular polarization resolved femtosecond transient absorption (fs-TA) measurements were conducted (Figure 4). In these measurements, pump and probe beams were circularly polarized and linearly polarized, respectively. Upon 1000 nm (E_{11}) excitation, the *R*-PDI-(6,5) film showed a sub-ps rise of SWCNT trion induced absorption (IA) at 1200 nm (Figure 4b), which can be attributed to the fast charge separation process in SWCNTs.[30, 31] Strong anisotropy to the circular polarization state of the pump beam was observed for both the E_{11} ground-state bleaching (GSB) peak (Figure 4a) and trion IA (Figure 4b). The TA anisotropy favors LCP excitation of the (6,5) E_{11}, which is in line with the CPL conductivity anisotropy observed in the CPL-TRMC measurements (Figure 3c). IA peaks from PDI anion around 700 nm are not pronounced significantly, indicating spin-dependent CS process is occurring solely in/between SWCNTs and PDI is not likely to be involved in the initial CS process.[32]

The impact of probe pulse polarization dependence was also examined, by controlling the polarization of the probe pulse to be the same as the pump pulse.(Figure S13) Upon 1020 nm excitation, quenching of the difference between the signal intensity in the CP excitation of the E_{22} GSB signal was observed upon this configuration, and this could be attributed to the cancellation between the difference in the absorbance and the evolution of the GSB signal upon CPL excitation, which strongly suggests that the origin of signal difference observed in polarization-uncontrolled probe measurements were not simply originated anisotropy in the absorbance of CP light.

Apart from the initial assumption that charge separation occurs between PDI and SWCNT, fs-TA results suggest that initial charge separation takes place within SWCNTs. Involvement of PDI in photophysical process in *R*-PDI-(6,5) was further investigated by washing *R*-PDI-(6,5)

samples by solvents. The removal of PDI from the surface of SWCNT was confirmed by Raman spectroscopy before/after the immersion processes into $CHCl_3$. The PDI showed specific vibrational peaks at 1297, 1377, and 1570 cm^{-1} (Figure S5a). Although *R*-PDI-(6,5) film showed peaks of both *R*-PDI and pristine SWCNT, the peaks from PDI (especially 1377 cm^{-1}) totally disappeared after the washing process at the boiling point of $CHCl_3$ for 2h, clearly suggesting the negligible residue of PDI in the washed film. CPL-TRMC results of the washed *R*-PDI-(6,5) film suggest that PDI does not contribute to the carrier dynamics measured by the 9 GHz probe, since E_{11} CPL excitation of the washed film yielded almost identical photoconductivity traces to those of the film before washing (Figure S8a). We also tried deposition of *S*-PDI which has opposite chirality to initially deposited *R*-PDI after washing, however, it did not induce any change in the photoconductivity traces (Figure S8b), still giving the inverted polarity in CPL-TRMC to the CD spectra. Addition of the R-PDI onto pristine (6,5) films with vapor deposition and drop-casting did not induce enhancement of CD of the E_{11} peak, which indicates the enhancement of this peak shown in Figure 1b is likely to be coming from the SWCNT film itself (Figure S3). Thus, we conclude that the spin-selectivity observed in CPL-TRMC upon E_{11} excitation of *R*-PDI-(6,5) film is originating from the charge separation within a SWCNT or in between adjacent SWCNT, but not from CS between SWCNT and PDI.

CPL dependency in CPL-TRMC and CPL resolved fs-TA was only observed in *R*-PDI-(6,5) upon E_{11} excitation, whereas pristine (11,-5) and *S*-PDI-(11,-5) did not show similar CPL dependence (Figure S7d-f). We may attribute the lack of CPL dependence observed in pristine (11,-5) and *S*-PDI-(11,-5) to the difference in CS pathways, where the inter-tubular CS is not activated in these films upon E_{11} excitation (Figure S6a-d). The linear polarization conductivity anisotropy in FP-TRMC in these films was estimated to be rather higher in 1020 nm (E_{11})

compared to 355 (E_{33}) excitations for both films, with the anisotropy of $\phi\Sigma\mu_{max}$ estimated as 7.1% and 18.3% for the pristine (11,-5) and 13.1% and 22.2% for S-PDI-(11,-5) film upon E_{33} and E_{11} excitations, respectively. The inversion of the polarity with attenuation was not observed for both of the pristine (11,-5) and *S*-PDI-(11,-5) films, indicating intra-tubular charge separation is predominant in these films upon E_{11} excitations. From these results, we conclude that facilitation of inter-tubular charge separation is the key in spin-selective CS behavior observed in *R*-PDI-(6,5) films upon E_{11} excitation. Since this behavior holds for films where the *R*-PDI has been removed from the heterojunction, this spin-selective CS behavior appears to be an inherent property of the (6,5) SWCNT film.

In conclusion, we established CPL-TRMC instrument and successfully probed the CP induced conductivity anisotropy of the *R*-PDI-(6,5) film. By using CPL-TRMC technique, we could observe inverted conductivity anisotropy to the CD originating from spin-dependent CS in SWCNT in *R*-PDI-(6,5) film upon E_{11} excitation. The origin of the spin-dependent behavior observed in CPL-TRMC was explained by activation of inter-tubular CS in SWCNT upon E_{11} excitation in contrast to the dominant intra-tubular CS upon E_{33} and E_{22} excitation, revealed by the linear polarization conductivity anisotropy in FP-TRMC and the fs-TA. The CPL-TRMC developed in the present work is expected to serve as a powerful tool for the ultra-fast screening of chiral molecular condensates as potential chiral electronic and spintronic materials in the future.

EXPERIMENTAL

(6,5) and (11,-5) SWCNTs were prepared by single-chirality enantiomer separation of CoMoCAT SWCNT using stepwise elution gel chromatography with triple surfactant system of sodium cholate, sodium dodecyl sulfate, and sodium lithocholate.[33-36] Randomly-oriented SWCNT films were deposited by vacuum filtration on filter membrane and transferred to quartz plates for optical measurements.[37,38] *R*- and *S*-PDI was synthesized by following a literature procedure.[10] The successful synthesis was confirmed by NMR (JEOL AL-400). Tetrahydrofuran (THF) was purchased from Nacalai Tesque and used without further purification. *R*/*S*-PDI films and SWCNT/PDI composite films were prepared by drop casting 50 μL of R/S-PDI 1mg/mL THF solution onto quartz plates and SWCNT films, respectively.

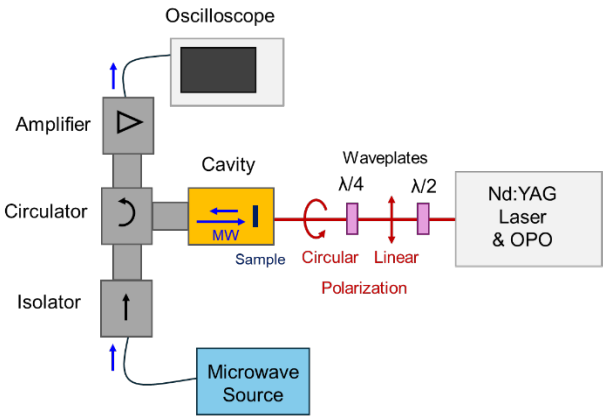

Figure 5. Schematics of CPL-TRMC setup. Nd/YAG lasers with optical parametric oscillator (OPO) are used for the excitation light sources at 355, 580 and 1020 nm. A Gunn diode oscillator or microwave signal generator was employed as a microwave source with the tuning range of 100kHz~43.5GHz at 1-100 mW.

FP-TRMC experiments were carried out as follows. For 355 nm pulsed photoinjection measurements, pulses were generated by third-harmonic generation with the photon density of

0.9×10^{15} photons cm^{-2} from Spectra-Physics INDI-HG Nd/YAG laser, operated with the pulse duration of 5-8 ns and 10 Hz). For 580 and 1020 nm pulsed photoinjection measurements, pulses were generated by the EKSPLA NT300 Nd/YAG laser, operated with the pulse duration of 3-5 ns and 10 Hz. The laser wavelength was tuned by the OPO to generate pulses with photon density of 3.0×10^{15} photons cm^{-2} and 5.2×10^{15} photons cm^{-2} for 580 and 1020 nm excitation pulse, respectively. The SWCNT or SWCNT/PDI sample was inserted to the X-band microwave cavity resonating with TE102 mode at ca. ~9.1 GHz from a Gunn diode oscillator or from a signal generator Rhode & Schwarz SMF 100A. The incident power of microwave was typically set at 3 mW, and the power reflection from the cavity was amplified and recorded with a MDO3024 oscilloscope and converted directly into the electric conductivity transients.

In both instrumental set-ups, linear polarization dependence was measured by introducing a cube polarizer and a half-waveplate into the excitation beam path to control the linear polarization. CPL-TRMC experiments were carried out by introducing a quarter waveplate to the linear polarization-dependent measurements to generate a circularly polarized beam. For all polarization-dependent measurements, conductivity transients were recorded as three sets of 512 traces averaging for each polarization by alternating polarization for every measurement and average values were taken. The schematic diagram of CPL-TRMC is shown in Figure 5.

Circular polarization-resolved femtosecond transient absorption (fs-TA) spectroscopy was conducted using a Coherent Libra Ti:sapphire laser, operated with an output of 800 nm at 1 kHz. A TOPAS optical parametric amplifier (OPA) generated 1020 nm pulses with pulse duration of ~150 fs. The pulse train was adjusted at 500 Hz through an optical chopper. White-light continuous probe pulses with a range of 500–1500 nm were generated via self-phase modulation by pumping a 1 cm thick sapphire crystal with an 800 nm pulse. Circularly polarized pump

pulses were generated by introduction of a quarter waveplate into the beam path. A Helios spectrometer (Ultrafast Systems) was used for collecting fs-TA spectra.[11, 15]

ASSOCIATED CONTENT

The following files are available free of charge.

Supporting Information. Experimental details of UV-vis-NIR; CD and Raman spectroscopy; additional experimental data of UV-vis-NIR, CD, and Raman spectroscopy; linear polarization dependent FP-TRMC; CPL-TRMC and fs-TA. (PDF)

AUTHOR INFORMATION

Notes

The authors declare no competing financial interests.

ACKNOWLEDGMENT

This work was supported by a Grant-in-Aid for Scientific Research (Grant Nos. 22H00314, 20H05862, 20H05867, JP23H00262, JP20H02573, JP21H05017, JP23H00259, JP23K23179, and JP24H01200), JST-CREST (Grant No. JPMJCR23O3) and JST-PRESTO (Grant No. JPMJPR21Q5), US-JAPAN PIRE collaboration (Grant No. JPJSJRP20221202), JST ASPIRE project (Grant No. JPMJAP2310) and JST FOREST, (Grant No. JPMJFR235Z), Japan. This work was authored in part by the National Renewable Energy Laboratory, operated by Alliance for Sustainable Energy, LLC, for the U.S. Department of Energy (DOE) under Contract No. DE-

AC36-08GO28308. NREL authors M.A.H-P. and J.L.B. were funded for fs-TA spectroscopy by the Solar Photochemistry Program, Division of Chemical Sciences, Geosciences, and Biosciences, Office of Basic Energy Sciences, U.S. DOE. The views expressed in the article do not necessarily represent the views of the DOE or the U.S. Government.

REFERENCES

(1) Ray, S.; Daube, S.; Leitus, G.; Vager, Z.; Naaman, R. Chirality-Induced Spin-Selective Properties of Self-Assembled Monolayers of DNA on Gold. *Phys. Rev. Lett.* **2006**, 96 (3), 036101.

(2) Kiran, V.; Mathew, S. P.; Cohen, S. R.; Hernández Delgado, I.; Lacour, J.; Naaman, R. Helicenes—A New Class of Organic Spin Filter. *Adv. Mater*. **2016**, 28 (10), 1957–1962.

(3) Bian, Z.; Kato, K.; Ogoshi, T.; Cui, Z.; Sa, B.; Tsutsui, Y.; Seki, S.; Suda, M. Hybrid Chiral MoS2 Layers for Spin-Polarized Charge Transport and Spin-Dependent Electrocatalytic Applications. *Adv. Sci.* **2022**, 9 (17), 2201063.

(4) Naaman, R.; Waldeck, D. H. Spintronics and Chirality: Spin Selectivity in Electron Transport through Chiral Molecules. *Annu. Rev. Phys. Chem.* **2015**, 66 (1), 263–281.

(5) Li, D.; Yu, G. Innovation of Materials, Devices, and Functionalized Interfaces in Organic Spintronics. *Adv. Func. Mater.* **2021**, 31 (28), 2100550.

(6) Tirion, S. H.; van Wees, B. J. Mechanism for Electrostatically Generated Magnetoresistance in Chiral Systems without Spin-Dependent Transport. *ACS nano* **2024**, 18 (8), 6028–6037.

(7) Liu, T.; Weiss, P. S. Spin Polarization in Transport Studies of Chirality-Induced Spin Selectivity. *ACS nano* **2023**, 17 (20), 19502–19507.

(8) Pierce, D. T.; Meier, F. Photoemission of Spin-Polarized Electrons from GaAs. *Phys. Rev. B* **1976**, 13 (12), 5484.

(9) Oiwa, A.; Mitsumori, Y.; Moriya, R.; Słupinski, T.; Munekata, H. Effect of Optical Spin Injection on Ferromagnetically Coupled Mn Spins in the III-V Magnetic Alloy Semiconductor (Ga, Mn) As. *Phys. Rev. Lett.* **2002**, 88 (13), 137202.

(10) Shang, X.; Song, I.; Ohtsu, H.; Lee, Y. H.; Zhao, T.; Kojima, T.; Jung, J. H.; Kawano, M.; Oh, J. H. Supramolecular Nanostructures of Chiral Perylene Diimides with Amplified Chirality for High-Performance Chiroptical Sensing. *Adv. Mater.* **2017**, 29 (21), 1605828.

(11) Hao, J.; Lu, H.; Mao, L.; Chen, X.; Beard, M. C.; Blackburn, J. L. Direct Detection of Circularly Polarized Light Using Chiral Copper Chloride–Carbon Nanotube Heterostructures. *ACS nano* **2021**, 15 (4), 7608–7617.

(12) Bloom, B. P.; Graff, B. M.; Ghosh, S.; Beratan, D. N.; Waldeck, D. H. Chirality Control of Electron Transfer in Quantum Dot Assemblies. *J. Am. Chem. Soc.* **2017**, 139 (26), 9038–9043.

(13) Eckvahl, H. J.; Tcyrulnikov, N. A.; Chiesa, A.; Bradley, J. M.; Young, R. M.; Carretta, S.; Krzyaniak, M. D.; Wasielewski, M. R. Direct Observation of Chirality-Induced Spin Selectivity in Electron Donor–Acceptor Molecules. *Science* **2023**, 382 (6667), 197–201.

(14) Das, T. K.; Tassinari, F.; Naaman, R.; Fransson, J. Temperature-Dependent Chiral-Induced Spin Selectivity Effect: Experiments and Theory. *J. Phys. Chem. C* **2022**, 126 (6), 3257–3264.

(15) Bindl, D. J.; Ferguson, A. J.; Wu, M.-Y.; Kopidakis, N.; Blackburn, J. L.; Arnold, M. S. Free Carrier Generation and Recombination in Polymer-Wrapped Semiconducting Carbon Nanotube Films and Heterojunctions. *J. Phys. Chem. Lett.* **2013**, 4 (21), 3550–3559.

(16) Seki, S.; Saeki, A.; Sakurai, T.; Sakamaki, D. Charge Carrier Mobility in Organic Molecular Materials Probed by Electromagnetic Waves. *Phys. Chem. Chem. Phys.* **2014**, 16 (23), 11093–11113.

(17) Saeki, A.; Koizumi, Y.; Aida, T.; Seki, S. Comprehensive Approach to Intrinsic Charge Carrier Mobility in Conjugated Organic Molecules, Macromolecules, and Supramolecular Architectures. *Acc. Chem. Res.* **2012**, 45 (8), 1193–1202.

(18) Seki, S.; Paitandi, R. P.; Choi, W.; Ghosh, S.; Tanaka, T. Electron Transport over 2D Molecular Materials and Assemblies. *Acc. Chem. Res.* **2024**, 57 (18), 2665–2677.

(19) Wei, X.; Tanaka, T.; Yomogida, Y.; Sato, N.; Saito, R.; Kataura, H. Experimental Determination of Excitonic Band Structures of Single-Walled Carbon Nanotubes Using Circular Dichroism Spectra. *Nat. Commun.* **2016**, 7 (1), 12899.

(20) Sato, N.; Tatsumi, Y.; Saito, R. Circular Dichroism of Single-Wall Carbon Nanotubes. *Phys. Rev. B* **2017**, 95 (15), 155436.

(21) O'connell, M. J.; Bachilo, S. M.; Huffman, C. B.; Moore, V. C.; Strano, M. S.; Haroz, E. H.; Rialon, K. L.; Boul, P. J.; Noon, W. H.; Kittrell, C.; others. Band Gap Fluorescence from Individual Single-Walled Carbon Nanotubes. *Science* **2002**, 297 (5581), 593–596.

(22) Dürkop, T.; Getty, S. A.; Cobas, E.; Fuhrer, M. Extraordinary Mobility in Semiconducting Carbon Nanotubes. *Nano Lett.* **2004**, 4 (1), 35–39.

(23) Shen, Y.; Reparaz, J. S.; Wagner, M. R.; Hoffmann, A.; Thomsen, C.; Lee, J.-O.; Heeg, S.; Hatting, B.; Reich, S.; Saeki, A.; others. Assembly of Carbon Nanotubes and Alkylated Fullerenes: Nanocarbon Hybrid towards Photovoltaic Applications. *Chem. Sci.* **2011**, 2 (11), 2243–2250.

(24) Ehli, C.; Oelsner, C.; Guldi, D. M.; Mateo-Alonso, A.; Prato, M.; Schmidt, C.; Backes, C.; Hauke, F.; Hirsch, A. Manipulating Single-Wall Carbon Nanotubes by Chemical Doping and Charge Transfer with Perylene Dyes. *Nat. Chem.* **2009**, 1 (3), 243–249.

(25) Bachilo, S. M.; Strano, M. S.; Kittrell, C.; Hauge, R. H.; Smalley, R. E.; Weisman, R. B. Structure-Assigned Optical Spectra of Single-Walled Carbon Nanotubes. *Science* **2002**, 298 (5602), 2361–2366.

(26) Huang, H.; Kajiura, H.; Maruyama, R.; Kadono, K.; Noda, K. Relative Optical Absorption of Metallic and Semiconducting Single-Walled Carbon Nanotubes. *J. Phys. Chem. B* **2006**, 110 (10), 4686–4690.

(27) Yan, L.; Xie, Y.; Mitzi, D. B.; Sercel, P. C.; Phillips, A. J.; Blackburn, J. L.; You, W. Giant Apparent Optical Circular Dichroism in Thin Films of Bismuth-Based Hybrid Organic–Inorganic Metal Halide Semiconductor Through Preferred Orientation. *Adv. Opt. Mater.* **2024**, 12 (13), 2302766.

(28) Kumamoto, Y.; Yoshida, M.; Ishii, A.; Yokoyama, A.; Shimada, T.; Kato, Y. Spontaneous Exciton Dissociation in Carbon Nanotubes. *Phys. Rev. Lett*. **2014**, 112 (11), 117401.

(29) Park, J.; Reid, O. G.; Blackburn, J. L.; Rumbles, G. Photoinduced Spontaneous Free-Carrier Generation in Semiconducting Single-Walled Carbon Nanotubes. *Nat. Commun.* **2015**, 6 (1), 8809.

(30) Sulas-Kern, D. B.; Zhang, H.; Li, Z.; Blackburn, J. L. Microsecond Charge Separation at Heterojunctions between Transition Metal Dichalcogenide Monolayers and Single-Walled Carbon Nanotubes. *Mater. Horiz.* **2019**, 6 (10), 2103–2111.

(31) Kang, H. S.; Sisto, T. J.; Peurifoy, S.; Arias, D. H.; Zhang, B.; Nuckolls, C.; Blackburn, J. L. Long-Lived Charge Separation at Heterojunctions between Semiconducting Single-Walled Carbon Nanotubes and Perylene Diimide Electron Acceptors. *J. Phys. Chem. C* **2018**, 122 (25), 14150–14161.

(32) Zeman IV, C. J.; Kim, S.; Zhang, F.; Schanze, K. S. Direct Observation of the Reduction of Aryl Halides by a Photoexcited Perylene Diimide Radical Anion. *J. Am. Chem. Soc.* **2020**, 142 (5), 2204–2207.

(33) Wei, X.; Tanaka, T.; Hirakawa, T.; Yomogida, Y.; Kataura, H. Determination of Enantiomeric Purity of Single-Wall Carbon Nanotubes Using Flavin Mononucleotide. *J. Am. Chem. Soc.* **2017**, 139 (45), 16068–16071.

(34) Wei, X.; Tanaka, T.; Hirakawa, T.; Tsuzuki, M.; Wang, G.; Yomogida, Y.; Hirano, A.; Kataura, H. High-Yield and High-Throughput Single-Chirality Enantiomer Separation of Single-Wall Carbon Nanotubes. *Carbon* **2018**, 132, 1–7.

(35) Yomogida, Y.; Tanaka, T.; Zhang, M.; Yudasaka, M.; Wei, X.; Kataura, H. Industrial-Scale Separation of High-Purity Single-Chirality Single-Wall Carbon Nanotubes for Biological Imaging. *Nat. Commun.* **2016**, 7 (1), 12056.

(36) Yomogida, Y.; Tanaka, T.; Tsuzuki, M.; Wei, X.; Kataura, H. Automatic Sorting of Single-Chirality Single-Wall Carbon Nanotubes Using Hydrophobic Cholates: Implications for Multicolor near-Infrared Optical Technologies. *ACS Appl. Nano Mater.* **2020**, 3 (11), 11289–11297.

(37) He, X.; Gao, W.; Xie, L.; Li, B.; Zhang, Q.; Lei, S.; Robinson, J. M.; Hároz, E. H.; Doorn, S. K.; Wang, W.; others. Wafer-Scale Monodomain Films of Spontaneously Aligned Single-Walled Carbon Nanotubes. *Nat. Nanotechnol.* **2016**, 11 (7), 633–638.

(38) Katsutani, F.; Gao, W.; Li, X.; Ichinose, Y.; Yomogida, Y.; Yanagi, K.; Kono, J. Direct Observation of Cross-Polarized Excitons in Aligned Single-Chirality Single-Wall Carbon Nanotubes. *Phys. Rev. B* **2019**, 99 (3), 035426.